1   # Metformin suppresses development of the

2   # *Echinococcus multilocularis* larval stage targeting

3   # the TOR pathway

4

5   Julia A. Loos[a,b,*], Valeria A. Dávila[a,b,*], Klaus Brehm[c], Andrea C. Cumino[a,b,d#]

6

7

8   [a] *Laboratorio de Zoonosis Parasitarias, Departamento de Biología, Facultad de Ciencias*

9   *Exactas y Naturales, Universidad Nacional de Mar del Plata (UNMdP), Funes 3350,*

10   *Nivel Cero, (7600) Mar del Plata, Argentina*

11   [b] *Consejo Nacional de Investigaciones Científicas y Técnicas (CONICET), Argentina.*

12   [c] *University of Würzburg, Institute of Hygiene and Microbiology, Josef-Schneider-Strasse*

13   *2, D-97080 Würzburg, Germany*

14   [d] *Departamento de Química, Facultad de Ciencias Exactas y Naturales, Universidad*

15   *Nacional de Mar del Plata (UNMdP), Funes 3350, Nivel 2, (7600) Mar del Plata,*

16   *Argentina*

17   **These authors contributed equally to this work. Author order was determined in order*

18   *of increasing seniority.*

19

20

21   Running title: Efficacy of metformin against *E. multilocularis*

22   [#]Address correspondence to Andrea C. Cumino, acumino@gmail.com

23

Abstract

Alveolar echinococcosis (AE) is a severe disease caused by the larval stage of the tapeworm *Echinococcus multilocularis*. Current chemotherapeutic treatment options based on benzimidazoles are of limited effectiveness, which underlines the need to find new anti-echinococcosis drugs. Metformin is an anti-hyperglycemic and anti-proliferative agent that shows activity against the related parasite *E. granulosus*. Hence, we assessed the *in vitro* and *in vivo* effects of the drug on *E. multilocularis*. Meformin exerted significant dose-dependent killing effects on *in vitro* cultured parasite stem cells and protoscoleces and significantly reduced the de-differentiation of protoscoleces into metacestodes. Likewise, oral administration of metformin (50 mg/kg/day for 8 weeks) was effective in achieving a significant reduction of parasite weight in a secondary murine AE model. Our results revealed mitochondrial membrane depolarization, activation of Em-AMPK, suppression of Em-TOR and overexpression of Em-Atg8 in the germinal layer of metformin-treated metacestode vesicles. The opposite effects on the level of active Em-TOR in response to exogenous insulin and rapamycin suggest that Em-TOR is part of the parasite's insulin signalling pathway. Finally, the presence of the key lysosomal pathway components, through which metformin reportedly acts, was confirmed in the parasite by *in silico* assays. Taken together, these results introduce metformin as a promising candidate for AE treatment. Although our study highlights the importance of those direct mechanisms by which metformin reduces parasite viability, it does not necessarily preclude any additional systemic effects of the drug that might reduce parasite growth *in vivo*.

2

Introduction

48

49   Alveolar echinococcosis (AE) is a zoonosis caused by the cestode *Echinococcus*

50   *multilocularis*, which is endemic in the Northern hemisphere (1, 2). This life-threatening disease

51   is of increasing public health concern, especially in Europe, China and Canada, where the parasite

52   became more prevalent (3, 4). The parasite is predominantly perpetuated in a sylvatic cycle, with

53   wild carnivores (mainly foxes) as definitive hosts and small mammals (usually rodents) as

54   intermediate hosts. Humans can accidentally acquire the infection through ingestion of parasite

55   eggs shed in the feces of a definite host. Once an individual is infected, *E. multilocularis* forms

56   metacestodes, which grow aggressively and infiltrate in the host tissue (primarily the liver), thus

57   causing AE (5). *E. multilocularis* metacestodes reproduce asexually by exogenous formation and

58   budding of daughter vesicles. They are composed of a complex germinal layer which contains

59   20-25% of stem cells (called germinative cells), the only proliferating cell type in the parasite and

60   the responsible for metastasis formation and continuous parasite growth (6).

61   Treatment alternatives for AE are systemic chemotherapy and/or surgery. Surgery

62   (radical or palliative) is complemented by post-operative pharmacotherapy (recommended in all

63   patients for at least two years, 7). In those cases where surgery is not feasible, chemotherapy

64   remains as the only option. Although there are alternative drugs, albendazole (ABZ) and

65   mebendazole are the only ones licensed to date. Both exhibit a relatively good clinical efficacy,

66   but are associated with adverse side effects and lack of parasiticidal activity (8, 9). Therefore, the

67   identification of better or alternative drugs becomes increasingly urgent (5).

68   One of the most promising approaches to find new compounds against neglected

69   infectious diseases is the repurposing of existing drugs (10). Metformin (Met, N, N-

70   dimethylbiguanide), an anti-hyperglycemic agent widely used in type 2 diabetes mellitus

71   treatment (11), has emerged as an anticancer drug, which is also effective against several

72   pathogens, including *Trichinella spiralis*, *Staphylococcus aureus*, *Pseudomonas aeruginosa*,

73   hepatitis B virus, hepatitis C virus and human immunodeficiency virus (HIV) (12, 13). The drug

74   has also been shown to suppress tumorsphere formation and to selectively target the cancer stem

75   cells (CSCs) of various tumour types both in *in vitro* cultures and in *in vivo* mouse experiments

76   (14-16).

77   The effects of Met can be partially attributed to AMPK (AMP-activated protein kinase)

78   activation, which depends on LKB1 (liver kinase B1) (17, 18). AMPK is a highly conserved

79   sensor of cellular energy charge that regulates various metabolic pathways (19). It was

80   demonstrated that Met treatment increases cellular levels of AMP through inhibition of complex

81   I of the electron transport chain, leading to inhibition of the mitochondrial function and activation

82   of AMPK (18). Nevertheless, recent studies showed that treatment of primary hepatocytes with

83   clinically relevant concentrations of Met, as well as chronic administration of 50 mg/kg/day in

84   mice, efficiently activates AMPK without disrupting the energy state (20). Thus, the mechanism

85   by which Met activates AMPK is not yet fully understood.

86   The anti-proliferative action of Met can be mediated by the indirect suppression of the

87   TOR (Target Of Rapamycin) pathway, mainly as a result of the activation of AMPK, and the

88   inactivation of IGF1R (Insulin-like growth factor type I receptor), two mechanisms that play a

89   critical role in cell proliferation and growth (15, 21, 22). In all eukaryotes, TOR kinase is found

90   in two functionally distinct complexes, TORC1 and TORC2 (23). TORC1 is a master regulator

91   of anabolic pathways and a key hub mediating control of cell growth in response to nutrients and,

92   in metazoans, to growth factors as well (insulin/IGF, which regulate the insulin–PI3K–AKT-

93   pathway) (23, 24). Thereby, Met leads to phosphorylation and activation of AMPK (Thr^{172}),

94   which in turn reduces the phosphorylation and activity of TOR (Ser^{2448}). Consequently,

95   expression/phosphorylation of TOR-downstream effectors such as ribosomal protein S6 kinase

96   (S6K, Thr^{389}), 4E-binding protein 1 (4EBP1, Thr$^{37/46}$) and IGF1R (Tyr$^{1135/6}$) is reduced, blocking

97   protein synthesis and inactivating the cell proliferation (15, 25, 26). On the other hand, Met has

98   been shown to activate AMPK and inhibit TOR by promoting the v-ATPase-Ragulator-

99   AXIN/LKB1-AMPK complex to assemble into the lysosome surface. The shutdown of TORC1

100   in turn promotes autophagy, a lysosomal process of bulk degradation of proteins and organelles

101   (23, 27).

102   Recently, we have observed a significant *in vitro* anti-parasitic effect of Met on *E.*

103 *granulosus* protoscoleces and metacestodes (28) and demonstrated that oral administration of this

104 drug was effective against the larval stage of the parasite in the murine cystic echinococcosis (CE)

105 infection model (29). In addition, we have described the indirect activation of Eg-AMPK in

106 response to Met treatment and showed that, in the parasite, the drug induces autophagy in the

107 same way as rapamycin, an inhibitor of TOR (28, 30, 31). Since AE and CE are two related

108 diseases that differ significantly regarding pathogenesis and metacestode morphology, it is of high

109 interest to assess Met efficacy also against *E. multilocularis*. Therefore, in this work, we assessed

110 the potential anti-parasitic effect of Met on *E. multilocularis* stem cell-containing primary cell

111 cultures as well as in a secondary mouse infection model of AE, and examined the effect of this

112 drug on mitochondrial function and the AMPK-TOR-autophagy pathway in the parasite. In

113 addition, we raised the question of whether Met controls the development of *Echinococcus*

114 through the indirect inhibition of TOR, as a consequence of the ATP synthesis inhibition, and/or

115 through the direct inhibition of TOR, by the lysosomal pathway.

116

117   **Materials and Methods**

118   **Ethics statement**

119   Female CF-1 mice (8 weeks of age) were supplied by the National Health Service and

120 Food Quality (SENASA), Mar del Plata, and housed in specific pathogen-free (SPF) facilities at

121 the bioterium of the National University of Mar del Plata (UNMdP). Experimental protocols for

122 using mice were evaluated and approved by the Animal Experimental Committee at the Faculty

123 of Exact and Natural Sciences, UNMdP (permit number: 2555-08-15). Experiments for the

124 continuous passage of *E. multilocularis* larval material in Mongolian jirds (*Meriones*

125 *unguiculatus*) were carried out in accordance with European and German regulations on the

126 protection of animals. Ethical approval of these studies was obtained from the local ethics

127 committee of the government of Lower Franconia (permit no. 55.2 DMS 2532-2-354).

128

129   **Maintenance, culture, and collection of parasites**

130   *E. multilocularis* (isolates J2012 and 8065) was maintained by serial intraperitoneal

131   passage in *Meriones unguiculatus* or CF-1 mice as described by Spiliotis and Brehm (32).

132   Homogenized metacestode material obtained from *M. unguiculatus* or CF-1 mice was cultured *in*

133   *vitro* with rat Reuber hepatoma or Huh7 cells as previously described (32). In addition,

134   protoscoleces obtained from CF-1 mice were cultured *in vitro* as in Wang et al. (33). Once

135   metacestode tissue or protoscoleces developed metacestode vesicles (typically after 1 to 3 months

136   of *in vitro* culture), they were collected and fixed for *in toto* immunolocalization assays with 4%

137   paraformaldehyde prepared in 0.1 M PBS (pH 7.4) as described by Loos et al. (30). *In vitro*

138   staining of metacestodes with JC-1 was performed by incubating the metacestode vesicles for 30

139   min in culture media in the presence of 10 mg/mL JC-1 (28). JC-1 is a positively charged

140   fluorescent compound that can penetrate mitochondria and change its color as a function of the

141   mitochondrial membrane potential ($\Delta\Psi$m). It accumulates as aggregates with intense red

142   fluorescence within the mitochondria when the $\Delta\Psi$m is high, or remains as green monomers in

143   the cytoplasm and the mitochondria when the $\Delta\Psi$m is low (34). Isolation of protoscoleces and

144   primary stem cell cultures were carried out as described by Spiliotis et al. (35).

145

146   **Drug treatment and viability assays**

147   Metformin (Sigma-Aldrich) was used dissolved in water at final concentrations of 1, 5

148   and 10 mM. Primary stem cells were cultivated in hepatocyte-conditioned medium (35)

149   supplemented with Met for 72 h, and the cell vitality was assessed by an alamar Blue assay (36).

150   Protoscoleces were incubated in medium 199 supplemented with Met for 8 days and viability was

151   subsequently assessed using a methylene blue staining assay (30). In all culture systems, medium

152   was changed every third day, including fresh addition of Met. All experiments were carried out

153   at least three times independently.

154

155   **Metacestode vesicles development in the presence of metformin**

156   *E. multilocularis* protoscoleces (50 µl for each condition) were cultured in RPMI 1640

157   medium (Gibco) containing 25 % (v/v) FBS (Gibco), 0.45 % (w/v) yeast extract, 0.4 % (w/v) of

158   glucose and 100 μg/ml penicillin, streptomycin and gentamicin in a 25 cm^2 culture flask at 37 ºC

159   in the presence of 5 % CO_2. The experimental conditions evaluated were control and 10 mM Met.

160   The medium was changed every 7 days, including fresh addition of Met. At the same time, each

161   culture was monitored under an optical microscope in order to record the total number of larval

162   vesicles. The experiment was repeated three times.

163

164   *In toto* **immunohistochemistry**

165   For *in toto* immunohistochemistry, control and treated protoscoleces and metacestode

166   vesicles were processed for analysis of total and phosphorylated (Thr^{174}) Em-AMPKα, Em-Atg8,

167   phosphorylated (Ser^{3122}) Em-TOR and Em-AKT, as previously described (28, 30, 31). The

168   samples were incubated with primary monoclonal antibodies directed against phosphorylated and

169   total human AMPKα (Phospho-AMPKα -Thr^{172}- (40H9) Rabbit mAb and AMPKα (D63G4)

170   Rabbit mAb, Cell Signalling cat no. 2535 and 5832, respectively, USA,1:1000 dilution), primary

171   polyclonal antibody directed against the N-terminus of human LC3 (MAP LC3β clone H-50,

172   Santa Cruz sc-28266, USA, 1:1000 dilution), primary monoclonal antibody directed against

173   phosphorylated human mTOR (Phospho-mTOR -Ser^{2448}- (D9C2) Rabbit mAb, Cell Signalling

174   cat no 5536, USA, 1:1000 dilution) and primary polyclonal antibody directed against total mouse

175   AKT (also known as PKB) (AKT antibody, Cell Signalling cat no. 9272, USA, 1:1000 dilution).

176   The anti-TOR antibody used in these assays is directed against an epitope which showed 30%

177   amino acid identity with the possible orthologs of *E. multilocularis* (Em-TOR) (GenBank

178   annotated as CDS40303, see alignment of conseverd motif in Fig. S2 B, red box). Negative

179   controls consisted of omission of primary antibody.

180   Immunofluorescence images were acquired using an inverted confocal laser scanning

181   microscope (Nikon, Confocal Microscope C1) with an excitation/emission wavelength of

182   494/517 nm for Alexa Fluor 488-conjugated antibodies and 536/617 nm for propidium iodide

183   stained nuclei. Fluorescence intensity was meassured using ImageJ software (NIH,

184   https://imagej.nih.gov/ij/, 37) in randomly chosen area sections of control and pharmacologically

185   treated samples. The surrounding background was subtracted before different regions of interest

7

186   (ROIs) were analyzed to obtain the mean intensity values. A total of 20 images per condition of

187   three independent sets of experiments were acquired and analyzed. Image files were loaded as

188   separate image stacks. Ratios of Em-AMPKα-P, Em-Atg8 or Em-TOR-P to nuclei fluorescence

189   intensity were calculated and displayed as bar plots. Negative controls consisted of omission of

190   primary antibody.

191

192   **Experimental animals and determination of efficacy of *in vivo* treatment**

193   Healthy CF-1 mice (30 ± 35 g) were acclimatized for one week before initiation of the

194   experiment. Mice were infected by intraperitoneal infection with 200 μl of homogenized

195   metacestode material (8065 strain) to produce experimental secondary AE (38). The animals were

196   maintained in standard polyethylene cages (three mice per cage), under controlled laboratory

197   conditions (temperature 20 ± 2ºC, 12 h photoperiod with lights off at 8.00 p.m., $50 \pm 5\%$

198   humidity). Food and water were provided *ad libitum*. Every 3 - 4 days per week, animals were

199   placed into a clean cage with fresh wood shavings. The pharmacological treatment was performed

200   by intragastric administration of a drug aqueous suspension (0.3 ml/animal). At the end of

201   experiments, mice were euthanized by cervical dislocation and previous anesthesia with

202   ketamine-xylazine (50 mg/kg/mouse – 5 mg/kg/mouse). All efforts were made to minimize

203   suffering. Minimum number of animals was used in each experiment. At necropsy, the peritoneal

204   cavity was opened, and the parasite tissues were carefully recovered and weighted. The efficacy

205   of treatment was calculated using the following formula: 100 x {(mean parasite weight of control

206   group)-(mean parasite weight of treated group)}/ (mean parasite weight of control group). In

207   addition, samples were processed for scanning electron microscopy (SEM) with a JEOL JSM-

208   6460LV electron microscope as previously described (30).

209

210   **Experimental treatment of *E. multilocularis*-infected mice with metformin**

211   At the time point of infection, 12 CF-1 mice were allocated into 2 experimental groups

212   (6 animals/group) as untreated control group (water) and Met-treated group (50 mg/kg/day). The

213   drug was applied by per oral gavage daily for 60 days. At the end of treatment period, animals

214   were euthanized and necropsied.

215

Sequence analysis of *Echinococcus* TOR and Ragulator complex

217   A BLAST search for homologs of TOR and the different components of the Ragulator

218   complex   in   the   *E.   multilocularis*   and   *E.   granulosus*   genome   databases

219   (http://www.sanger.ac.uk/Projects/Echinococcus, 39) was performed using orthologs from *Homo*

220   *sapiens*,   *Fasciola hepatica*, *Hymenolepis microstoma*, *Drosophila hydei*, *Schistosoma*

221   *haematobium* and *Drosophila busckii* as queries. This search allowed the identification of the

222   putative orthologous genes encoding TOR and the Ragulator subunits (Em-*lamtor*1, Em-*lamtor*2,

223   Em-*lamtor*3, Em-*lamtor*4 and Em-*lamtor*5) whose predicted open reading frames were analyzed.

224   Orthologs were selected based on reciprocal best BLAST hits (40, 41) on an E-value cut-off of

225    $1e^{-25}$ and on the presence of the characteristic domains in the deduced amino acid sequences.

226   Sequence   alignments   were   generated   with   the   CLUSTALX   software   program

227   (https://www.ebi.ac.uk/Tools/msa/clustalo/) and the modeling of secondary structures of the

228   putative proteins was obtained from the deduced primary structures using the Gen-THREADER

229   (http://bioinf.cs.ucl.ac.uk/psipred/psiform.html).   The   SWISS-MODEL   server

230   (https://swissmodel.expasy.org/interactive) was used to generate alignments and homology

231   models for Em-TOR and Em-Ragulator proteins selecting template protein structures in PDB with

232   a high coverage (> 60% of target aligned to template) and sequence identity >30%. Also,

233   phosphorylation sites were predicted for Em-TOR by submitting the sequence to web-based tools

234   namely NetPhos 3.1 Server (http://www.cbs.dtu.dk/services/NetPhos).

235

Statistics

237   Data within experiments were compared using the Student's t-test or the non-parametric

238   Mann-Whitney test, and differences among groups were considered as statistically significant

239   significance with a p-value below 0.05. Statistical analyses were performed using R software

240   (https://www.R-project.org).

9

241

Results

Pharmacological sensitivity of *E. multilocularis* primary stem cells and protoscoleces to metformin

To study drug effects on parasite stem cells, we made use of the previously established primary cell culture system in which parasite cells are directly isolated from *in vitro* cultivated metacestode vesicles (35). These primary cell cultures are strongly enriched (up to 80%) in germinative stem cells (6). In order to investigate the *in vitro* effect of Met on the viability of these stem cell cultures, the percentage of living cells in response to different concentrations of Met was analyzed. Exposure to the drug for 72 h led to a dose-dependent decrease in the viability of primary cells, with significant effects at 5 mM or higher concentrations. After treatment with 10 mM Met, the viability percentage reached values below 50% (Figure 1A). Since secondary echinococcosis can be induced by de-differentiating protoscoleces (33, 42), drug effects were also assessed on this larval stage. As shown in Fig. S1A, Met exerted a dose-dependent effect on the viability of protoscoleces after 8 days of incubation. The mortality rate of protoscoleces reached 20, 40 and 60% with 1, 5 and 10 mM Met, respectively. Furthermore, the drug partially arrested the *in vitro* de-differentiation of protoscoleces into metacestode vesicles (Figure 1B).

Molecular changes induced by metformin in *E. multilocularis* larval stage

To explore the possible inhibitory effect of Met on the complex 1 of the respiratory chain, we studied the mitochondrial functional status using the membrane potential indicator JC-1 in *E. multilocularis* metacestodes vesicles (34).

Control and Met-treated metacestodes were examined by confocal microscopy for JC-1 fluorescence (Figure 2a, b). Following 48 h treatment with 10 mM Met, the relative values of red/green JC-1 fluorescence ratios showed low dispersion. At this point, untreated metacestodes showed a red/green fluorescence ratio with a mean value of 2.2, whereas Met treated metacestodes showed a lower mean ratio of around 0.7 (Figure 2c). Met treatment induced an increase in

268   depolarized regions indicated by the disappearance of red fluorescence and an increase in green

269   fluorescence (Figure 2b).

270   Since the maintenance of the $\Delta\Psi$m is required for ATP production, Met might activate

271   Em-AMPK as a consequence of cellular energy charge depletion (increased cellular AMP:ATP

272   ratio). Therefore, after confirming the expression of genes encoding the three subunits of AMPK

273   in *E. multilocularis* (28), we studied the phosphorylation at Thr^{176} of Em-AMPKα (AMPKα-P^{176})

274   as a read-out of its activation state. To this end, *in toto* immunolocalization assays using a

275   monoclonal antibody directed against the phosphorylated form of AMPKα were performed from

276   protoscoleces (Fig. S1B) and *in vitro* generated metacestodes (Figure 2d, e). As shown in Figs.

277   S1C and 2f, a significant increase in the Em-AMPKα-P^{176} level was observed after 48 h of

278   treatment with 10 mM Met, indicating Em-AMPKα activation under this condition. The

279   expression of Em-AMPKα-P^{176} was detected both in the nucleus and in the cytoplasm of the cells

280   of Met-treated and control samples, although in Met-treated parasites the nuclear expression was

281   higher than in the control condition. This is consistent with the presence of a nuclear export

282   sequence at the C-terminus of the catalytic subunit of Em-AMPK and its direct involvement in

283   transcriptional regulation. The fluorescence pattern was not observed when the parasites were

284   incubated with the secondary antibody alone (data not shown).

285   Since activation of AMPK by Met has been shown to induce autophagy (31, 43, 44), we

286   further examined the effects of the drug on the autophagic pathway in the larval stage of *E.*

287   *multilocularis*. By *in toto* immunolocalization assays, Em-Atg8 (a LC3β-homolog) was detected

288   in a diffuse and punctate form in both control (Figure 2g) and 10 mM Met treated metacestodes

289   (Figure 2h), with total fluorescence signal and the amount of punctuated structures being higher

290   in presence of the drug (Figure 2i). It should be added that under the effect of the drug the signal

291   was evidenced in the nucleus of germinal layer cells (Figure 2h).

292

293   **Pharmacological activation of Em-TOR in *E. multilocularis* larval stage**

294   In an attempt to determine the mechanism responsible for the anti-parasitic effect of Met,

295   its effect on TOR signaling was assessed. As TOR is activated by AKT phosphorylation at Ser^{2448}

11

296   to promote protein synthesis and cell proliferation (45), we used a phospho-specific antibody to

297   assess Em-TOR activity. As shown in Figure 3, 10 mM Met treatment resulted in inhibition of

298   Em-TOR, as demonstrated by decreased phosphorylation of Em-TOR (Ser[3122]) in treated

299   metacestodes (Figure 3Ad), compared with untreated metacestodes (Figure 3Aa). Additionally,

300   while treatment with Rp also caused inhibition of Em-TOR (Figure 3Ac), treatment with insulin

301   resulted in increased phosphorylation of Em-TOR[S3122] (Figure 3Ab). Importantly, we showed that

302   Ser[3122] is highly conserved in the parasite protein, including the region around the serine (Fig.

303   S2).

304   Subsequently, we analyzed the immunolocalization of Em-AKT, which was previously

305   reported by Hemer et al. (46), in the larval stage of *Echinococcus* because it may be involved in

306   the post-translational regulation of Em-TOR (Fig. S1D). The expression of total Em-AKT was

307   detected in the tegument of control and Met-treated protoscoleces (Fig. S1Da, c). However, its

308   expression was generalized and with a spotted pattern in insulin-treated protoscoleces (Fig.

309   S1Db). While the expression level of this kinase was unchanged in parasites treated with Met, it

310   was increased in samples treated with insulin (Fig. S1E).

311

312   **Anthelmintic efficacy of metformin on secondary alveolar echinococcosis in mice**

313   Given our results showing the *in vitro* effects of Met on primary stem cell viability and

314   the ability of protoscoleces to de-differentiate into metacestodes, we examined whether this drug

315   could affect parasite growth *in vivo*. Each mouse was intraperitoneally infected with 200 μl of

316   metacestode tissue and Met was administrated daily orally at 50 mg/kg/day for 60 days. All mice

317   survived at the end of the experiment and Met did not affect the animal weight and diet

318   consumption. As shown in Figure 4A, Met was effective in achieving a significant reduction of

319   parasite weight (1.5 ± 1.1 g) compared to the untreated group (3.14 ± 1.1 g).

320   To analyze the ultrastructural changes of parasite material recovered from each

321   experimental group, SEM studies were performed. Metacestode tissue from control mice

322   appeared with protoscoleces and an intact germinal layer (Figure 4Ba-c). In contrast,

323 metacestodes collected from Met-treated mice displayed a marked reduction in the number of

324 germinal cells (Figure 4Bd-f).

325

326 ***In silico* analysis of key components of the TOR pathway in *Echinococcus***

327   Previously, by demonstrating sensitivity to rapamycin, induction of autophagy and

328 transcriptional expression of TOR in the larval stage of *E. granulosus*, the ocurrence of Em-TOR

329 in *E. multilocularis* was suggested (30, 47). The full-length open reading frame of Em-TOR,

330 identified by a BLAST search, predicts a protein of 3273 amino acids (annotated as CDS40303

331 and EmuJ_000787900 in the GenBank and GeneDB database, respectively) with 28-37% overall

332 identity to human TOR (P42345). The Em-TOR has a conserved domain structure containing N-

333 terminal HEAT (Huntington, EF3A, ATM, TOR) repeats followed by a FAT (FRAP, ATM,

334 TTRAP) domain (~600 residue), the FRB (FKBP-rapalog binding) domain (~100 residue), the

335 kinase domain, and a FATC domain (~35 residue) at the C-terminus (Fig. S2A). Although the N-

336 terminal HEAT repeat and FAT region show a relatively low grade of conservation in the primary

337 sequence (24-43 and 25-37% identity, respectively) with respect to vertebrate TOR orthologs, the

338 C-terminal FRB domain, the kinase domain, and the FATC domain are highly conserved (46-

339 70% identity) (Fig. S2). As in the human TOR, the FRB domain and the putative regulatory

340 domain (RD) of Em-TOR are arranged on either side of the catalytic site (Fig. S2A, B). The RD

341 is referred to as the negative regulatory domain (residues 2430–2492 in human TOR), since its

342 deletion leads to an increase in TOR activity (48, 49). The mammalian amino acid sequence of

343 this region is highly conserved, structurally disordered (PDB ID 4JSV) and contains regulatory

344 phosphorylation sites such as Thr^{2446} and Ser^{2448} ([KRSRTR<u>T</u>D<u>S</u>YSAGQSVE]), which aligned

345 with a conserved motif in Em-TOR (Fig. S2; 50, 51). Prediction of phosphorylation hotspot

346 regions using NetPhos 3 revealed a score of 0.93 for Thr^{3119} and Ser^{3122}, suggesting that these two

347 putative phosphorylation sites match the TRT-X1/2-S consensus sequence. Finally, Em-TOR

348 showed a considerable similarity in secondary and tertiary structures to human TOR (PDB 6bcu.1.

349 A, 52).

13

350   Subsequently, the occurrence of the five subunits of Ragulator (LAMTOR1-5) was also

351   analyzed in *E. multilocularis*. Extensive BLAST searches on the parasite genome revealed five

352   genes coding for the different subunits of Ragulator (Figs. S3 and S4). The genes encode a 166-

353   amino acid protein (named Em-LAMTOR1 and annotated as CDS42462 and EmuJ_001017100

354   in the GenBank and GeneDB database respectively), a 125-amino acid protein (named Em-

355   LAMTOR2 and annotated as CDS41091 and EmuJ_000871100 in the GenBank and GeneDB

356   database respectively), a 110-amino acid protein (named Em-LAMTOR3 and annotated as

357   CDS43561 and EmuJ_001132600 in the GenBank and GeneDB database respectively), a 121-

358   amino acid protein (named Em-LAMTOR4 and annotated as CDS38220 and EmuJ_000555600

359   in the GenBank and GeneDB database respectively) and a 103-amino acid protein (named Em-

360   LAMTOR5 and annotated as CDS43359 and EmuJ_001111300 in the GenBank and GeneDB

361   database respectively).

362   The predicted Em-LAMTOR1 sequence aligned with 23 and 30% identity with the *H.*

363   *sapiens* (NP_060377) and *F. hepatica* (THD24342) orthologs, respectively. The Em-LAMTOR1

364   subunit contains elements that support the identification of the protein product as a member of

365   the LAMTOR family. The predicted protein is similar in size to the human and *F. hepatica*

366   proteins. Likewise, it is predicted to be helix-rich (42%) and has two N-terminal cysteines that

367   may be sites for S-acylation (palmitoylation). In addition, Em-LAMTOR1 contains conserved

368   key residues for its interaction with the other components of the complex (Fig. S4A). On the other

369   hand, Em-LAMTOR2 aligned with 36 and 63% identity with the *H. sapiens* (NP_054736) and *H.*

370   *microstoma* (CDS27935) orthologs, respectively. The Em-LAMTOR2 subunit contains a

371   conserved Roadblock/LC7 domain (pfam03259) located in the middle of the protein (Fig. S4B).

372   For its part, the Em-LAMTOR3 subunit showed 24 % identity with the *H. sapiens* (NP_068805)

373   ortholog and it presents the mitogen-activated protein kinase kinase 1 interacting (pfam08923)

374   (Fig. S4C). Additionally, the predicted Em-LAMTOR4 sequence aligned with 34 and 37%

375   identity with the *H. sapiens* (NP_001008396) and *S. haematobium* (XP_012797450) orthologs,

376   respectively (Fig. S4D). Finally, the Em-LAMTOR5 subunit showed 27 and 18 % identity with

377   the *H. sapiens* (O43504) and *D. busckii* (XP_017851496) orthologs, respectively and it contains

14

378   the Roadblock/LC7 domain (pfam03259) like Hs-LAMTOR5 (Fig. S4E). Lastly, homology

379   modeling results showed that Em-LAMTOR1, Em-LAMTOR2, Em-LAMTOR3 and Em-

380   LAMTOR4 proteins have similar quaternary structure to that of human orthologs in the Ragulator

381   complex (PDB 6ehr.1 and 5yk3.3, PDB 5x6v.1, PDB 5yk3.1 and PDB 5y39.1, respectively).

382

383   **Discussion**

384   The severe infection caused by the *E. multilocularis* metacestode is currently treated with

385   benzimidazoles. However, these drugs are ineffective for some patients, at least in part due to

386   their low bioavailability, limited half-life in the host and restricted uptake by the parasite.

387   Moreover, they also lack parasiticidal activity and cause toxicity (9, 53). In this report, we

388   demonstrated that Met reduces *E. multilocularis* primary stem cell viability in culture and parasite

389   mass in a murine secondary AE model. The drug toxicity mechanism could be attributed to the

390   mitochondrial membrane depolarization and the modulation of the AMPK-TOR-autophagy

391   pathway in the parasite. Importantly, both the *in vitro* and *in vivo* models and the treatment

392   schedule that we used for the screening of Met against AE have been previously established (32,

393   38, 54).

394   Met not only significantly decreased the viability of primary stem cells and protoscoleces,

395   but also reduced the de-differentiation of protoscoleces into metacestode vesicles. These findings

396   are consistent with results showing that the drug inhibited stem cell proliferation in a dose-

397   dependent manner in preclinical cancer models (14). The concentrations of Met used in our *in*

398   *vitro* experiments are high as compared to those in plasma (5-18 μM) and liver (50-100 μM)

399   reported *in vivo* (55). However, they are within the range used to examine the *in vitro* effects of

400   the drug on cell metabolism and proliferation (56, 57). A likely cause for the need of these drug

401   concentrations is the high amount of glucose and growth factors employed in culture media (58).

402   *Echinococcus* stem cell targeting using Met could lead to a breakthrough of therapeutic

403   approaches for AE, given that it has been suggested that the stem cells are resistant to ABZ (59,

404   60). In fact, compared to other drugs with *in vitro* effect on parasite stem cells, such as kinase

405   inhibitors (61, 62), Met can also control the parasite development *in vivo*. In relation to this, it has

15

406   been reported that Met can act on stem cells through the PKA-GSK3β signal pathway by

407   suppressing the expression of KLF5 (Krüppel-like factor 5), a transcription factor involved in the

408   expression of developmental genes (57), which has a putative ortholog in the *Echinococcus*

409   genome (Em_000425100).

410   In our *in vivo* assay, treatment with Met showed a significant therapeutic effect against

411   murine experimental AE. Under this condition, a reduction in the weight of the recovered

412   metacestodes as well as the destruction of their germinal layer, were observed. Considering that

413   germinative cells can be released into the environment of the parasite and affect neighbouring

414   organs, our *in vitro* results, together with the results showing ultrastructural changes induced by

415   Met *in vivo*, suggest that the drug may not only be effective in preventing metastasis formation,

416   but also be useful for its administration during the peri and postoperative periods, in which cell

417   spread could occur. This could be reinforced by the ability of Met to weaken the induction or

418   reverse the epithelial-mesenchymal transition (EMT) in cancer-like cells (63). It is important to

419   note that the dose of Met employed in this experiment is the lowest used in mice (50 mg/kg/day)

420   and is within the clinically relevant range for humans (64). Met has a bioavailability of 50-60%,

421   it is not metabolized, and its mean plasma half-life is approximately 20 h (55, 65). After oral

422   ingestion, Met is absorbed by the small intestine, distributed by the portal vein and concentrates

423   in the liver (65). This could be an advantage for the AE treatment since the liver is the main target

424   organ of the parasite. In fact, Met accumulation in *E. granulosus* has been reported in the

425   experimental CE (29). Currently, we are extending the study to evaluate the *in vivo* efficacy of

426   Met using different infection and treatment schemes, by increasing the parasitic inoculum and

427   starting the treatment later.

428   Concomitantly, our results showed that in germinative cells of metacestodes, Met would

429   inhibit the complex I of the mitochondrial respiratory chain (Figure 2a-c), a direct molecular target

430   confirmed for the drug (58). Therefore, by altering the mitochondrial metabolism and oxidative

431   phosphorylation, Met could affect the production of ATP and TCA cycle intermediates,

432   preventing the proliferation of germinative cells, as has been reported for cancer stem cells (15).

433   The strategy of interfering with the energy-generating systems in the larval stage of *E.*

16

434   *multilocularis* has previously been proven to be effective using drugs such as buparvaquone and

435   quinazoline-type compounds *in vitro* (10, 66).

436   On the other hand, as a consequence of ATP depletion, Met activates AMPK and inhibits

437   TOR. The latter is a key mediator of the PI3K/AKT pathway, which responses to growth factors

438   and insulin (17). Although in the *E. multilocularis* genome project it has already been reported

439   that the parasite encodes a TOR ortholog and an insulin-like tyrosine kinase receptor (InsR) (39),

440   no studies concerning the TOR activity in the parasite have been performed to date. In our

441   experiments, Met led to the activation of Em-AMPK and the decrease in Em-TOR activity in both

442   metacestode vesicles and protoscoleces. The inhibition of Em-TOR could justify the anti-

443   echinococcal effect of this drug on the parasite's larval stage, as has been evidenced in cancer

444   cells (15). In addition, the reduction in Em-TOR phosphorylation after Met treatment was

445   accompanied by an increase in Em-Atg8 levels, indicating autophagy induction. Since it has been

446   described that Met can activate pro-death autophagy in lymphoma and melanoma cells (43, 44),

447   the anti-echinococcal effects of Met could also be partially dependent on autophagy.

448   Although the main building blocks of insulin-InsR-PI3K-AKT-FoxO-TOR pathway are

449   generally conserved among mammals and invertebrates, *Echinococcus* spp. possesses a single

450   gen for InsR, FoxO, S6K and EIF4B (similar to flies and free-living worms), and lacks of insulin-

451   like peptides, PTEN, TSC1/2 and Rheb (30, 31, 39, 46, 67). Given that host insulin stimulates the

452   *in vitro* vesicular growth of *E. multilocularis* (46, 68) and TOR represents a direct target of the

453   InsR-PI3K-AKT pathway in insulin-stimulated cells, we also assessed the potential differential

454   phosphorylation of Em-TOR in response to exogenous insulin and rapamycin (a direct inhibitor

455   of TOR), demonstrating that Em-TOR reacts oppositely under these stimuli. Thus, we confirmed

456   that Em-TOR is part of the parasite signalling pathway downstream of insulin provided by the

457   host. Similar to its orthologs, Em-TOR is a high molecular-weight protein that contains all

458   conserved structural domains. It also contains, between the catalytic and FATC domains, two

459   conserved phosphorylation hotspots, Thr^{3119} and Ser^{3122} (corresponding to the phosphosites Thr^{2446}

460   and Ser^{2448} in human TOR), which respond to insulin (48, 50). Phosphorylation of these sites is

461   highly conserved among vertebrate species but is absent in free-living invertebrates (69).

462   However, we showed that the phosphorylation site region is partially conserved in helminth

463   parasites, demonstrating that the phosphorylation status of Em-TOR can be measured by using

464   antibodies against the phosphorylated Hs-TOR-S^{2448} form. Probably as a result of the coevolution

465   of the parasite and its vertebrate host, TOR activity in these helminths could be regulated in the

466   same way as in vertebrates (46, 70). Moreover, in these TOR sequences, we identified additional

467   peptides previously unobserved, with coil structures, surrounding the phosphorylation sites into

468   RD. These sites may be druggable, providing new opportunities for the development of specific

469   inhibitors with a high degree of specificity for parasite TOR kinase.

470   On the other hand, intrigued by the discovery that Met may directly act on the lysosomal

471   pathway to promote AMPK activation and TOR inhibition (27, 55), we sought to establish the

472   presence of LAMTOR orthlogs in the *Echinococcus* genome. This finding, as well as the presence

473   of a gene encoding v-ATPase (71) and two Axin paralogs in the genome of this tapeworm (72),

474   suggest that the formation of the v-ATPase-Ragulator-AXIN / LKB1-AMPK complex is possible

475   in the parasite. This, added to the demonstration of the lysosomal pathway functionality within

476   the invertebrate model *C. elegans* (73), emphasizes the relevance of studying this pathway to

477   identify new pharmacological targets.

478   Although our study highlights the importance of the direct mechanims by which Met

479   reduces the parasite viability, we consider that Met could also have systemic effects that

480   contribute to its potential as an anti-echinococcal therapeutic agent *in vivo*. These may include

481   suppression of Warburg effect, a metabolic strategy acquired by *Echinococcus* larval stage under

482   limited oxygen supply (29, 74), and control of liver chronic inflammation, by reducing the

483   proinflammatory cytokine levels (75) and increasing the cytotoxic response by blocking PD-

484   1/PD-L1 (Programmed cell Death-1/Programmed Death Ligand-1) axis (76).

485   By targeting germinative cells, Met holds great promise for the treatment of AE.

486   Therefore, our results provide a rationale basis for testing the combination of Met and ABZ, given

487   that drugs with different mechanisms of action could improve treatment efficacy. On the other

488   hand, the drug presents the advantages of being commercially available, approved by the FDA,

489   and extensively characterized in terms of bioavailability and pharmacokinetics, with a good long-

490   term safety profile and controllable side-effects (13, 16).

491

506

507 References

508   1. Deplazes P, Eckert J. 2001. Veterinary aspects of alveolar echinococcosis—a zoonosis of

509   public health significance. Vet Parasitol 98:65-87.

510   2. Deplazes P, Rinaldi L, Alvarez Rojas CA, Torgerson PR, Harandi MF, Romig, T,

511   Antolova D, Schurer JM, Lahmar S, Cringoli G, Magambo J. 2017. Global distribution

512   of alveolar and cystic echinococcosis. Adv Parasitol 95:315-493.

513   3. Thompson A, Deplazes P, Lymbery AJ. 2017. *Echinococcus* and Echinococcosis, Part A,

514   Adv Parasitol, 95, Academic Press, p.525.

515 4. Trotz-Williams LA, Mercer NJ, Walters JM, Wallace D, Gottstein B, Osterman-Lind E,
516   Boggild AK, Peregrine AS. 2017. Public health follow-up of suspected exposure to
517   *Echinococcus multilocularis* in southwestern Ontario. Zoonoses Public Health 64:460-
518   467.

519 5. Kern P, Menezes da Silva A, Akhan O, Müllhaupt B, Vizcaychipi KA, Budke C, Vuitton
520   DA. 2017. The echinococcoses: diagnosis, clinical management and burden of disease.
521   Adv Parasitol 96:259-369.

522 6. Koziol U, Rauschendorfer T, Zanon Rodríguez L, Krohne G, Brehm K. 2014. The unique
523   stem cell system of the immortal larva of the human parasite *Echinococcus multilocularis*.
524   Evodevo 5:10.

525 7. Wen H, Vuitton L, Tuxun T, Li J, Vuitton DA, Zhang W, McManus DP. Echinococcosis:
526   Advances in the 21st Century. Clin Microbiol Rev 32:e00075-18.

527 8. Küster T, Kriegel N, Boykin DW, Stephens CE, Hemphill A. 2013. *In vitro* and *in vivo*
528   activities of dicationic diguanidino compounds against *Echinococcus multilocularis*
529   metacestodes. Antimicrob Agents Chemother 57:3829-3835.

530 9. Lundström-Stadelmann B, Rufener R, Ritler D, Zurbriggen R, Hemphill A. 2019. The
531   importance of being parasiticidal… an update on drug development for the treatment of
532   alveolar echinococcosis. FAWPAR 15:e00040.

533 10. Rufener R, Dick L, D'Ascoli L, Ritler D, Hizem A, Wells TN, Hemphill A, Lundström-
534   Stadelmann B. 2018. Repurposing of an old drug: *In vitro* and *in vivo* efficacies of
535   buparvaquone against *Echinococcus multilocularis*. Int J Parasitol Drugs Drug Resist
536   8:440-450.

537 11. Palmer SC, Strippoli GFM. 2018. Metformin as first-line treatment for type 2 diabetes.
538   Lancet 392:120.

539 12. Pierotti MA, Berrino F, Gariboldi M, Melani C, Mogavero A, Negri T, Pasanisi P, Pilotti
540   S. 2013. Targeting metabolism for cancer treatment and prevention: metformin, an old
541   drug with multi-faceted effects. Oncogene 32:1475-87.

542   13. Malik F, Mehdi SF, Ali H, Patel P, Basharat A, Kumar A, Ashok F, Stein J, Brima W,

543   Malhotra P, Roth J. 2018. Is metformin poised for a second career as an antimicrobial?.

544   Diabetes Metab Res Rev 34: e2975.

545   14. Hirsch HA, Iliopoulos D, Tsichlis PN, Struhl K. 2009. Metformin selectively targets

546   cancer stem cells, and acts together with chemotherapy to block tumor growth and

547   prolong remission. Cancer Res 69:7507-7511.

548   15. Mogavero A, Maiorana MV, Zanutto S, Varinelli L, Bozzi F, Belfiore A, Volpi CC,

549   Gloghini A, Pierotti MA, Gariboldi M. 2017. Metformin transiently inhibits colorectal

550   cancer cell proliferation as a result of either AMPK activation or increased ROS

551   production. Sci Rep 7:15992.

552   16. Kim JH, Lee KJ, Seo Y, Kwon JH, Yoon JP, Kang JY, Lee HJ, Park SJ, Hong SP, Cheon

553   JH, Kim WH, II Kim T. 2018. Effects of metformin on colorectal cancer stem cells

554   depend on alterations in glutamine metabolism. Sci Rep 8:409.

555   17. Shaw RJ, Lamia KA, Vasquez D, Koo SH, Bardeesy N, Depinho RA, Montminy M,

556   Cantley LC. 2005. The kinase LKB1 mediates glucose homeostasis in liver and

557   therapeutic effects of metformin. Science. 310:1642-1646.

558   18. Foretz M, Guigas B, Bertrand L, Pollak M, Viollet B. 2014. Metformin: from mechanisms

559   of action to therapies. Cell Metab 20:953-966.

560   19. Hardie DG. 2014. AMPK—sensing energy while talking to other signaling pathways.

561   Cell Metab 20:939-952.

562   20. He L, Wondisford FE. 2015. Metformin action: concentrations matter. Cell Metab

563   21:159-162.

564   21. Gwinn DM, Shackelford DB, Egan DF, Mihaylova MM, Mery A, Vasquez DS, Turk BE,

565   Shaw RJ. 2008. AMPK phosphorylation of raptor mediates a metabolic checkpoint. Mol

566   Cell 30:214-226.

567   22. Rozengurt E, Sinnett-Smith J, Kisfalvi K. 2010. Crosstalk between insulin/insulin-like

568   growth factor-1 receptors and G protein-coupled receptor signaling systems: a novel

569   target for the antidiabetic drug metformin in pancreatic cancer. Clin Cancer Res 16:2505-

570   2511.

571   23. Soulard A, Cohen A, Hall MN. 2009. TOR signaling in invertebrates. Curr Opin Cell Biol

572   21:825-836.

573   24. Lawrence RE, Zoncu R. 2019. The lysosome as a cellular centre for signalling,

574   metabolism and quality control. Nat Cell Biol 21:133-142.

575   25. Ma XM, Blenis J. 2009. Molecular mechanisms of mTOR-mediated translational control.

576   Nat Rev Mol Cell Biol 10:307-318.

577   26. Kato H, Sekine Y, Furuya Y, Miyazawa Y, Koike H, Suzuki K. 2015. Metformin inhibits

578   the proliferation of human prostate cancer PC-3 cells via the downregulation of insulin-

579   like growth factor 1 receptor. Biochem Biophys Res Commun 461:115-121.

580   27. Zhang CS, Li M, Ma T, Zong Y, Cui J, Feng JW, Wu YQ, Lin SY, Lin SC. 2016.

581   Metformin activates AMPK through the lysosomal pathway. Cell Metab 24:521-522.

582   28. Loos JA, Cumino AC. 2015. *In vitro* anti-echinococcal and metabolic effects of

583   metformin involve activation of AMP-activated protein kinase in larval stages of

584   *Echinococcus granulosus*. PLoS One 10:e0126009.

585   29. Loos JA, Dávila VA, Rodrígues CR, Petrigh R, Zoppi JA, Crocenzi FA, Cumino AC.

586   2017. Metformin exhibits preventive and therapeutic efficacy against experimental cystic

587   echinococcosis. PLoS Negl Trop Dis 11:e0005370.

588   30. Loos JA, Caparros PA, Nicolao MC, Denegri GM, Cumino AC. 2014. Identification and

589   pharmacological induction of autophagy in the larval stages of *Echinococcus granulosus*:

590   an active catabolic process in calcareous corpuscles. Int J Parasitol 44:415-427.

591   31. Loos JA, Nicolao MC, Cumino AC. 2018. Metformin promotes autophagy in

592   *Echinococcus granulosus* larval stage. Mol Biochem Parasitol 224:61-70.

593   32. Spiliotis M, Brehm K. 2009. Axenic *in vitro* cultivation of *Echinococcus multilocularis*

594   metacestode vesicles and the generation of primary cell cultures. Methods Mol Biol

595   470:245-262.

596   33. Wang H, Li J, Guo B, Zhao L, Zhang Z, McManus DP, Wen H, Zhang W. 2016. *In vitro*

597   culture of *Echinococcus multilocularis* producing protoscoleces and mouse infection with

598   the cultured vesicles. Parasit Vectors 9:411.

599   34. Reers M, Smith TW, Chen LB. 1991. J-aggregate formation of a carbocyanine as a

600   quantitative fluorescent indicator of membrane potential. Biochemistry 30:4480-4486.

601   35. Spiliotis M, Lechner S, Tappe D, Scheller C, Krohne G, Brehm K. 2008. Transient

602   transfection of *Echinococcus multilocularis* primary cells and complete *in vitro*

603   regeneration of metacestode vesicles. Int J Parasitol 38:1025-1039.

604   36. Anoopkumar-Dukie S, Carey JB, Conere T, O'sullivan E, Van Pelt FN, Allshire A. 2005.

605   Resazurin assay of radiation response in cultured cells. Br J Radiol 78:945-947.

606   37. Rangarajan S, Bone NB, Zmijewska AA, Jiang S, Park DW, Bernard K, Locy ML, Ravi

607   S, Deshane J, Mannon RB, Abraham E, Darley-Usmar V. 2018. Metformin reverses

608   established lung fibrosis in a bleomycin model. Nat Med 24:1121-1127.

609   38. Wang J, Jebbawi F, Bellanger AP, Beldi G, Millon L, Gottstein B. 2018. Immunotherapy

610   of alveolar echinococcosis via PD-1/PD-L1 immune checkpoint blockade in mice.

611   Parasite Immunol 40:e12596.

612   39. Tsai IJ, Zarowiecki M, Holroyd N, Garciarrubio A, Sanchez-Flores A, Brooks KL,

613   Tracey A, Bobes RJ, Fragoso G, Sciutto E, Aslett M, Beasley H, Bennett HM, Cai J,

614   Camicia F, Clark R, Cucher M, De Silva N, Day TA, Deplazes P, Estrada K, Fernández

615   C, Holland PWH, Hou J, Hu S, Huckvale T, Hung SS, Kamenetzky L, Keane JA, Kiss F,

616   Koziol U, Lambert O, Liu K, Luo X, Luo Y, Macchiaroli N, Nichol S, Paps J, Parkinson

617   J, Pouchkina-Stantcheva N, Riddiford N, Rosenzvit M, Salinas G, Wasmuth JD,

618   Zamanian M, Zheng Y, Taenia solium Genome Consortium, Cai X, Soberón X, Olson

619   PD, Laclette JP, Brehm K, Berriman M. 2013. The genomes of four tapeworm species

620   reveal adaptations to parasitism. Nature 496:57-63.

621   40. Doolittle RF. 1995. The multiplicity of domains in proteins. Annu Rev Biochem 64:287-

622   314.

623   41. Tatusov RL, Koonin EV, Lipman DJ. 1997. A genomic perspective on protein families.

624   Science 278:631-637.

625   42. Brehm K. 2010. The role of evolutionarily conserved signalling systems in *Echinococcus*

626   *multilocularis* development and host–parasite interaction. Med Microbiol Immunol

627   199:247-59.

628   43. Tomic T, Botton T, Cerezo M, Robert G, Luciano F, Puissant A, Gounon P, Allegra M,

629   Bertolotto C, Bereder JM, Tartare-Deckert S, Bahadoran P, Auberger P, Ballotti R,

630   Rocchi S. 2011. Metformin inhibits melanoma development through autophagy and

631   apoptosis mechanisms. Cell Death Dis 2:e199.

632   44. Shi WY, Xiao D, Wang L, Dong LH, Yan ZX, Shen ZX, Chen SJ, Chen Y, Zhao WL.

633   2012. Therapeutic metformin/AMPK activation blocked lymphoma cell growth via

634   inhibition of mTOR pathway and induction of autophagy. Cell Death Dis 3:e275.

635   45. Saini KS, Loi S, de Azambuja E, Metzger-Filho O, Saini ML, Ignatiadis M, Dancey JE,

636   Piccart-Gebhart MJ. 2013. Targeting the PI3K/AKT/mTOR and Raf/MEK/ERK

637   pathways in the treatment of breast cancer. Cancer Treat Rev 39:935-946.

638   46. Hemer S, Konrad C, Spiliotis M, Koziol U, Schaack D, Förster S, Gelmedin V,

639   Stadelmann B, Dandekar T, Hemphill A, Brehm K. 2014. Host insulin stimulates

640   *Echinococcus multilocularis* insulin signalling pathways and larval development. BMC

641   Biol 12:5.

642   47. Cumino AC, Lamenza P, Denegri GM. 2010. Identification of functional FKB protein in

643   *Echinococcus granulosus*: Its involvement in the protoscolicidal action of rapamycin

644   derivates and in calcium homeostasis. Int J Parasitol 40:651-661.

645   48. Sekulić A, Hudson CC, Homme JL, Yin P, Otterness DM, Karnitz LM, Abraham RT.

646   2000. A direct linkage between the phosphoinositide 3-kinase-AKT signaling pathway

647   and the mammalian target of rapamycin in mitogen-stimulated and transformed cells.

648   Cancer Res 60:3504-3513.

649   49. Baretić D, Berndt A, Ohashi Y, Johnson CM, Williams RL. 2016. Tor forms a dimer

650   through an N-terminal helical solenoid with a complex topology. Nat Commun 7:11016.

24

651   50. Navé BT, Ouwens M, Withers DJ, Alessi DR, Shepherd PR. 1999. Mammalian target of

652   rapamycin is a direct target for protein kinase B: identification of a convergence point for

653   opposing effects of insulin and amino-acid deficiency on protein translation. Biochem J

654   344 Pt 2:427-431.

655   51. Cheng SW, Fryer LG, Carling D, Shepherd PR. 2004. Thr2446 is a novel mammalian

656   target of rapamycin (mTOR) phosphorylation site regulated by nutrient status. J Biol

657   Chem 279:15719-15722.

658   52. Yang H, Jiang X, Li B, Yang HJ, Miller M, Yang A, Dhar A, Pavletich NP. 2017.

659   Mechanisms of mTORC1 activation by RHEB and inhibition by PRAS40. Nature

660   552:368-373.

661   53. Cotting J, Zeugin T, Steiger U, Reichen J. 1990. Albendazole kinetics in patients with

662   echinococcosis: delayed absorption and impaired elimination in cholestasis. Eur J Clin

663   Pharmacol 38:605-608.

664   54. Siles-Lucas M, Hemphill A. 2002. Cestode parasites: application of *in vivo* and *in vitro*

665   models for studies on the host-parasite relationship. Adv Parasitol 51:133-230.

666   55. Vancura A, Bu P, Bhagwat M, Zeng J, Vancurova I. 2018. Metformin as an anticancer

667   agent. Trends Pharmacol Sci 39:867-878.

668   56. Miller RA, Chu Q, Xie J, Foretz M, Viollet B, Birnbaum MJ. 2013. Biguanides suppress

669   hepatic glucagon signalling by decreasing production of cyclic AMP. Nature 494:256-

670   260.

671   57. Shi P, Liu W, Tala, Wang H, Li F, Zhang H, WuY, Kong Y, Zhou Z, Wang C, Chen W,

672   Liu R, Chen C. 2017. Metformin suppresses triple-negative breast cancer stem cells by

673   targeting KLF5 for degradation. Cell Discov 3:17010.

674   58. Wheaton WW, Weinberg SE, Hamanaka RB, Soberanes S, Sullivan LB, Anso E,

675   Glasauer A, Dufour E, Mutlu GM, Budigner GS, Chandel NS. 2014. Metformin inhibits

676   mitochondrial complex I of cancer cells to reduce tumorigenesis. Elife 3:e02242.

25

677   59. Schubert A, Koziol U, Cailliau K, Vanderstraete M, Dissous C, Brehm K. 2014.
678   Targeting *Echinococcus multilocularis* stem cells by inhibition of the Polo-like kinase
679   EmPlk1. PLoS Negl Trop Dis 8:e2870.

680   60. Brehm K, Koziol U. 2014. On the importance of targeting parasite stem cells in anti-
681   echinococcosis drug development. Parasite 21:72.

682   61. Hemer S, Brehm K. 2012. *In vitro* efficacy of the anticancer drug imatinib on
683   *Echinococcus multilocularis* larvae. Int J Antimicrob Agents 40:458-462.

684   62. Joekel DE, Lundström-Stadelmann B, Müllhaupt B, Hemphill A, Deplazes P. 2018.
685   Evaluation of kinase-inhibitors nilotinib and everolimus against alveolar echinococcosis
686   *in vitro* and in a mouse model. Exp Parasitol 188:65-72.

687   63. Qu C, Zhang W, Zheng G, Zhang Z, Yin J, He Z. 2014. Metformin reverses multidrug
688   resistance and epithelial–mesenchymal transition (EMT) via activating AMP-activated
689   protein kinase (AMPK) in human breast cancer cells. Mol Cell Biochem 386:63-71.

690   64. Graham GG, Punt J, Arora M, Day RO, Doogue MP, Duong JK, Furlong TJ, Greenfield
691   JR, Greenup LC., Kirkpatrick CM, Ray JE, Timmins P, Williams KM. 2011. Clinical
692   pharmacokinetics of metformin. Clin Pharmacokinet 50:81-98.

693   65. Wilcock C, Bailey CJ. 1994. Accumulation of metformin by tissues of the normal and
694   diabetic mouse. Xenobiotica 24:49-57.

695   66. Matsumoto J, Sakamoto K, Shinjyo N, Kido Y, Yamamoto N, Yagi K, Miyoshi H,
696   Nonaka N, Katakura K, Kita K, Oku Y. 2008. Anaerobic NADH-fumarate reductase
697   system is predominant in the respiratory chain of *Echinococcus multilocularis*, providing
698   a novel target for the chemotherapy of alveolar echinococcosis. Antimicrob Agents
699   Chemother 52:164-170.

700   67. Santos Pereira-Dutra F, Cancela M, Valandro Meneghetti B, Bunselmeyer Ferreira H,
701   Mariante Monteiro K, Zaha A. 2019. Functional characterization of the translation
702   initiation factor eIF4E of *Echinococcus granulosus*. Parasitol Res:1-13.

703   68. Konrad C, Kroner A, Spiliotis M, Zavala-Góngora R, Brehm K. 2003. Identification and

704   molecular characterisation of a gene encoding a member of the insulin receptor family in

705   *Echinococcus multilocularis*. Int J Parasitol. 33:301-312.

706   69. Copp J, Manning G, Hunter T. 2009. TORC-specific phosphorylation of mammalian

707   target of rapamycin (mTOR): phospho-Ser2481 is a marker for intact mTOR signaling

708   complex 2. Cancer Res 69:1821-1827.

709   70. Förster S, Koziol U, Schäfer T, Duvoisin R, Cailliau K, Vanderstraete M, Dissous C,

710   Brehm K. 2019. The role of fibroblast growth factor signalling in *Echinococcus*

711   *multilocularis* development and host-parasite interaction. PLoS Negl Trop Dis

712   13:e0006959.

713   71. Zheng H, Zhang W, Zhang L, Zhang Z, Li J, Lu G, Zhu Y, Wang Y, Huang Y, Liu J,

714   Kang H, Chen J, Wang L, Chen A, Yu S, Gao Z, Jin L, Gu W, Wang Z, Zhao L, Shi B,

715   Wen H, Lin R, Jones MK, Brejova B, Vinar T, Zhao G, McManus DP, Chen Z, Zhou Y,

716   Wang S. 2013. The genome of the hydatid tapeworm *Echinococcus granulosus*. Nat

717   Genet 45:1168-1175.

718   72. Montagne J, Preza M, Castillo E, Brehm K, Koziol U. 2019. Divergent Axin and GSK-3

719   paralogs in the beta-catenin destruction complexes of tapeworms. Dev Genes Evol

720   229:89-102.

721   73. Chen J, Ou Y, Li Y, Hu S, Shao LW, Liu Y. 2017. Metformin extends *C. elegans* lifespan

722   through lysosomal pathway. Elife 6:e31268.

723   74. Parkinson J, Wasmuth JD, Salinas G, Bizarro CV, Sanford C, Berriman M, Ferreira HB,

724   Zaha A, Blaxter ML, Maizels RM, Fernández C. 2012. A transcriptomic analysis of

725   *Echinococcus granulosus* larval stages: implications for parasite biology and host

726   adaptation. PLoS Negl Trop Dis 6: e1897.

727   75. Hirsch HA, Iliopoulos D, Struhl K. 2013. Metformin inhibits the inflammatory response

728   associated with cellular transformation and cancer stem cell growth. Proc Natl Acad Sci

729   USA 110:972-977.

730   76. Cha JH, Yang WH, Xia W, Wei Y, Chan LC, Lim SO, Li CW, Kim T, Chang SS, Lee

731   HH, Hsu JL, Wang HL, Kuo CW, Chang WC, Hadad S, Purdie CA, McCoy AM, Cai S,

732   Tu Y, Litton JK, Mittendorf EA, Moulder SL, Symmans WF, Thompson AM, Piwnica-

733   Worms H, Chen CH, Khoo KH, Hung MC. 2018. Metformin promotes antitumor

734   immunity via endoplasmic-reticulum-associated degradation of PD-L1. Mol Cell 71:606-

735   620.

736

737   **Figure legends**

738   **Figure 1.** *In vitro* effect of metformin on viability of primary stem cells of *E. multilocularis* and

739   on the de-differentiation process of protoscoleces to metacestodes. (A) Viability of primary cells

740   incubated in absence (C) or presence of different concentrations of metformin (1, 5 and 10 mM)

741   for 72 h. Triton 1% was used as positive control. Data are the mean ± S.D. of three independent

742   experiments. *Statistically significant difference ($P < 0.05$) compared with control. (B) Box plot

743   showing the number of metacestode vesicles per field of view recorded from untreated (C) and

744   Met-treated (10 mM) protoscolex cultures at day 7. *Statistically significant difference ($p < 0.05$)

745   compared with control. *n* shows number of images analysed.

746

747   **Figure 2.** Molecular effects of metformin on *in vitro* generated *E. multilocularis* metacestodes.

748   (a-c) Changes in mitochondrial membrane potential. (a, b) Representative confocal images

749   showing JC-1 fluorescence in metacestodes incubated under control conditions (a) or treated with

750   10 mM metformin (b) for 48 h. Bars indicate 200 μm. (c) Box plot graph showing the values of

751   the red/green JC-1 fluorescence ratios measured in control (C) and metformin (Met) treated

752   metacestodes by Image J Software. *Statistically significant difference ($P < 0.05$) compared with

753   control. (d-f) Pharmacological activation of Em-AMPKα. (d, e) Representative confocal images

754   of *in toto* immunolocalization assays revealed with an antibody conjugated with Alexa 488-green

755   fluorescence- and counterstained with propidium iodide -red fluorescence-. Control (d) and Met

756   treated metacestodes (e) incubated with anti-AMPKα-P antibody. Cytoplasmic expression is

757   observed in green. Nuclear expression is observed in yellow/orange, corresponding to the merged

758   fluorescences. Inset images correspond to transmission microscopy. Bars indicate 200 μm. (f)

759   Graph depicts the ratio of p-AMPKα to nuclei fluorescence intensity in metacestodes treated with

760   10 mM Met relative to controls. Values are expressed as means ± SEM (*p < 0.05 compared to

761   control). (g-i) Pharmacological induction of autophagy. (g, h) Representative confocal images of

762   *in toto* immunolocalization assays revealed with an antibody conjugated with Alexa 488 –green

763   fluorescence- and counterstained with propidium iodide -red fluorescence-. Control (g) and Met-

764   treated metacestodes (h) incubated with anti-LC3 antibody. Inset images correspond

765   totransmission microscopy. Bars indicate 200 μm. (i) Graph depicts the ratio of Em-Atg8 to nuclei

766   fluorescence intensity in metacestodes treated with 10 mM Met relative to controls. Values are

767   expressed as means ± SEM (*p < 0.05 compared to control).

768

769   **Figure 3.** Detection and immunolocalization of an activated form of Em-TOR in

770   pharmacologically treated *E. multilocularis* metacestodes. (A) Representative confocal images of

771   *in toto* immunolocalization assays revealed with an antibody conjugated with Alexa 488 -green

772   fluorescence- and counterstained with propidium iodide -red fluorescence-. Control (a) and

773   insulin (b), rapamycin (c) and metformin (d) treated metacestodes incubated with anti-TOR-P.

774   Inset images correspond to transmission microscopy. Bars indicate 200 μm. (B) Graph depicts the

775   ratio of Em-TOR-P^{S3122} to nuclei fluorescence intensity in metacestodes treated with 1U/ml

776   insulin (Ins), 10 μM rapamycin (Rp) and 10 mM metformin (Met) relative to controls (C). Values

777   are expressed as means ± SEM (*p < 0.05 compared to control).

778

779   **Figure 4.** *In vivo* efficacy of metformin against *E. multilocularis* larva stage. Box plot showing

780   the comparative distribution of the weight (g) of cysts recovered from untreated (C) and

781   metformin-treated (Met, 50 mg/kg/d) mice. A significant cyst weight reduction (*p < 0.05) was

782   achieved in treated animals. (B) Representative SEM images of cysts recovered from untreated

783   control mice (a-c) compared with Met-treated mice (d-f). Bars indicate: 50 μmin (a, d), 20 μm in
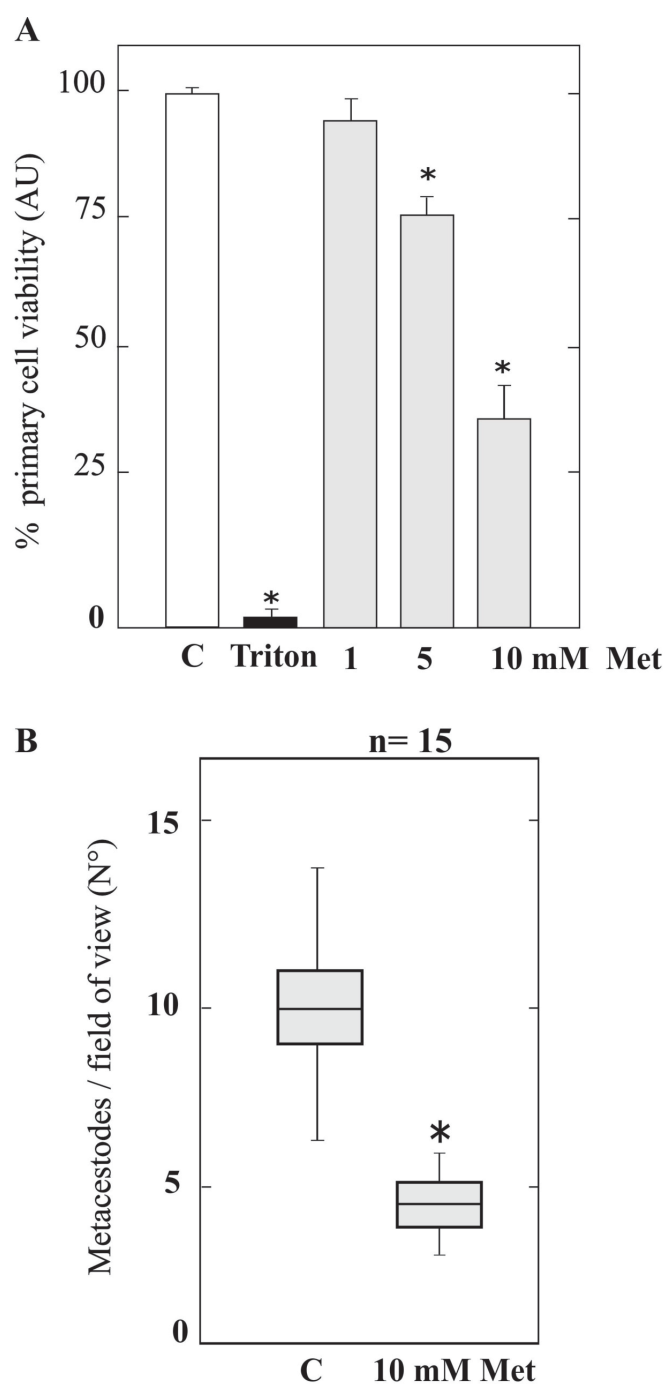
784   (b, e) and 10 μm in (c, f).

785

29

Figure 1. In vitro effect of metformin on viability of primary stem cells of E. multilocularis and on the de-differentiation process of protoscoleces to metacestodes. (A) Viability of primary cells incubated in absence (C) or presence of different concentrations of metformin (1, 5 and 10 mM) for 72 h. Triton 1% was used as positive control. Data are the mean ± S.D. of three independent experiments. *Statistically significant difference ($P < 0.05$) compared with control. (B) Box plot showing the number of metacestode vesicles per field of view recorded from untreated (C) and Met-treated (10 mM) protoscolex cultures. *Statistically significant difference ($p < 0.05$) compared with control. n shows number of images analysed.
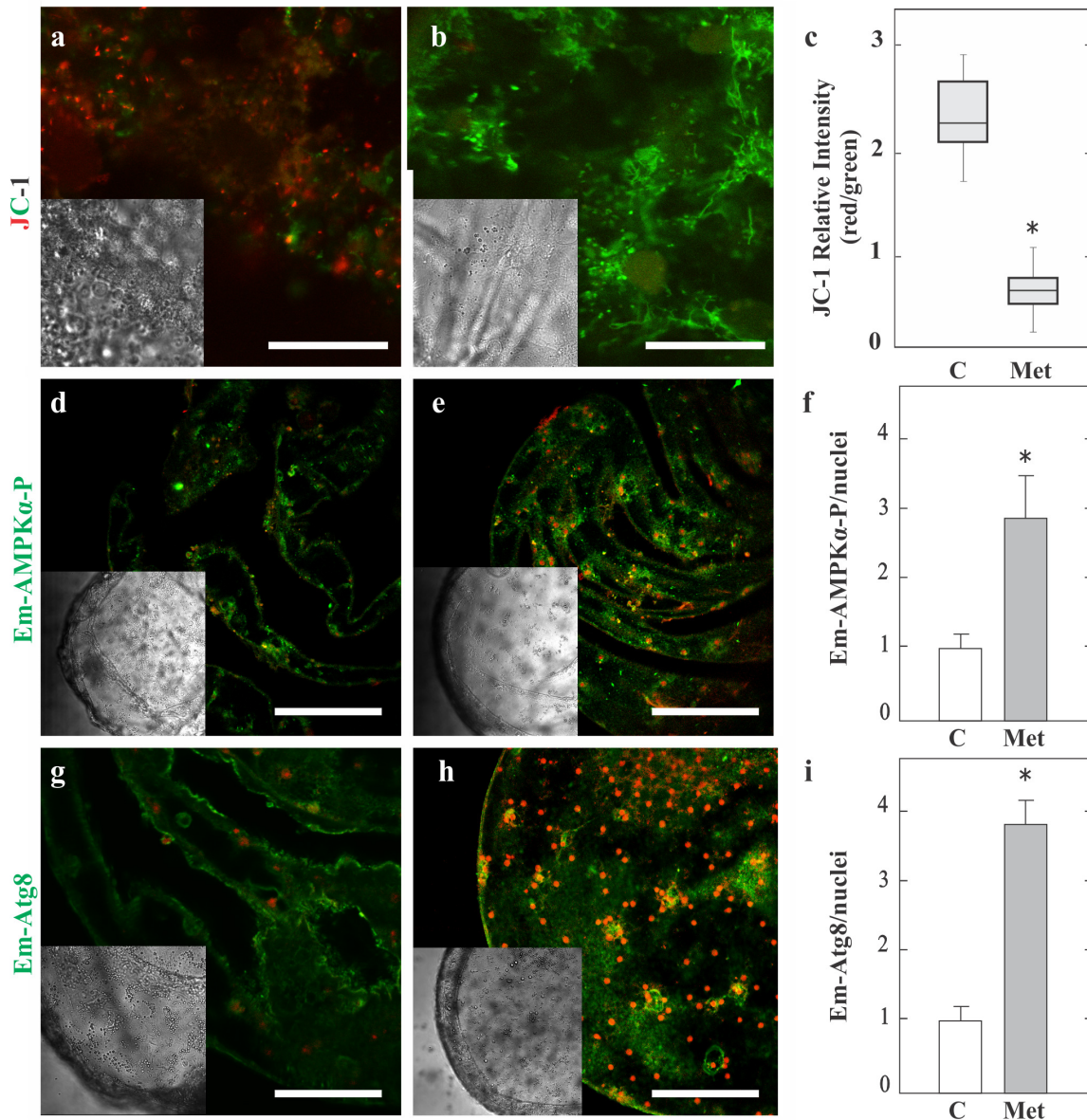
Figure 2. Molecular effects of metformin on in vitro generated *E. multilocularis* metacestodes. (a-c) Changes in mitochondrial membrane potential. (a, b) Representative confocal images showing JC-1 fluorescence in metacestodes incubated under control conditions (a) or treated with 10 mM metformin (b) for 48 h. Bars indicate 200 um. (c) Box plot graph showing the values of the red/green JC-1 fluorescence ratios measured in control (C) and metformin (Met) treated metacestodes by Image J Software. *Statistically significant difference (p<0.05) compared with control. (d-f) Pharmacological activation of Em-AMPK?. (d, e) Representative confocal images of in toto immunolocalization assays revealed with an antibody conjugated with Alexa 488-green fluorescence- and counterstained with propidium iodide -red fluorescence-. Control (d) and Met treated metacestodes (e) incubated with anti-AMPK?-P antibody. Cytoplasmic expression is observed in green. Nuclear expression is observed in yellow/orange, corresponding to the merged fluorescences. Inset images correspond to transmission microscopy. Bars indicate 200 um. (f) Graph depicts the ratio of p-AMPK? to nuclei fluorescence intensity in metacestodes treated with 10 mM Met relative to controls. Values are expressed as means ± SEM (*p < 0.05 compared to control). (g-i) Pharmacological induction of autophagy. (g, h) Representative confocal images of in toto immunolocalization assays revealed with an antibody conjugated with Alexa 488 -green fluorescence- and counterstained with propidium iodide -red fluorescence-. Control (g) and Met-treated metacestodes (h) incubated with anti-LC3 antibody. Inset images correspond to transmission microscopy. Bars indicate 200 um. (i) Graph depicts the ratio of Em-Atg8 to nuclei fluorescence intensity in metacestodes treated with 10 mM Met relative to controls. Values are expressed as means ± SEM (*p < 0.05 compared to control).
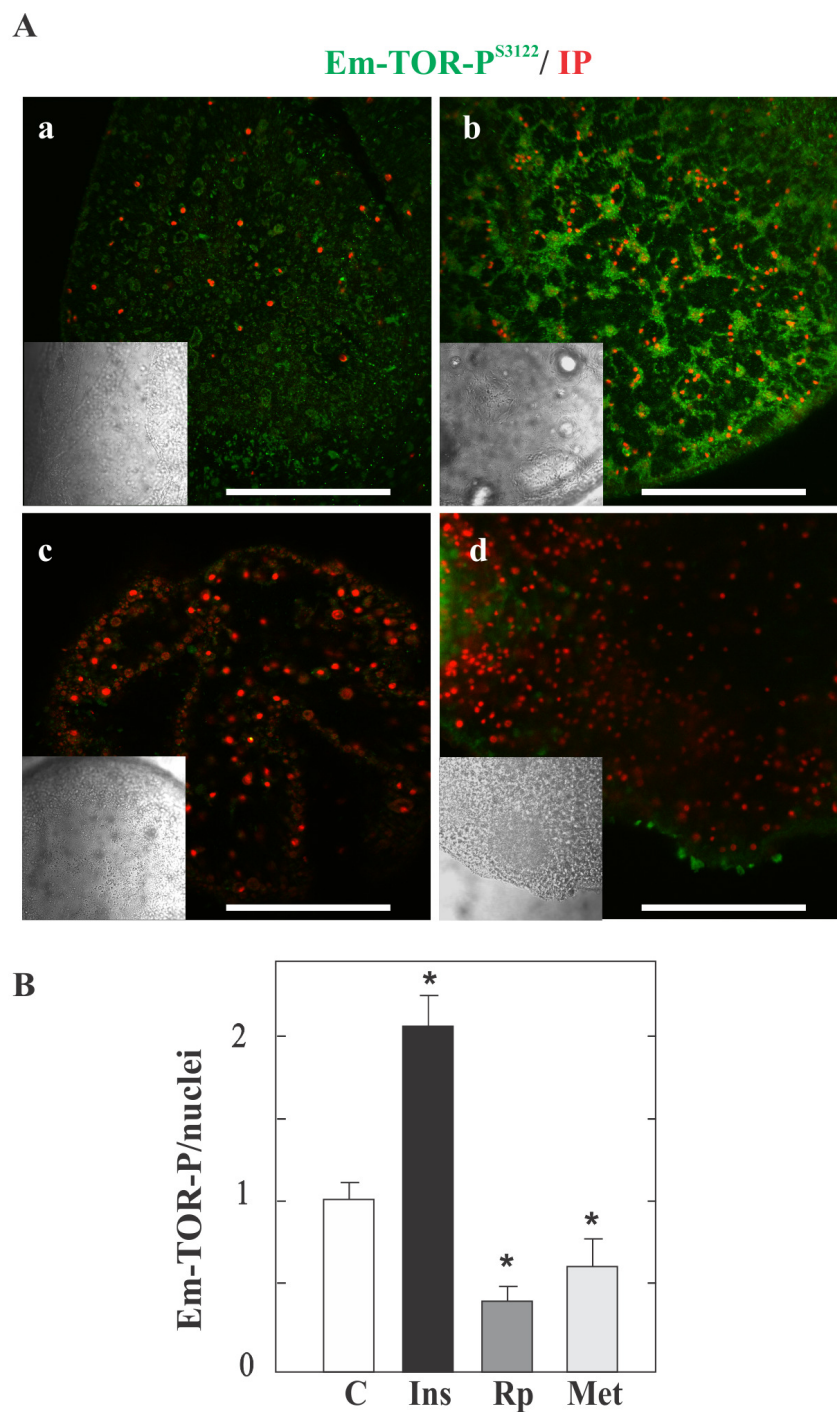
A

Em-TOR-P^{S3122}/ IP

Figure 3. Detection and immunolocalization of an activated form of Em-TOR in pharmacologically treated *E. multilocularis* metacestodes. (A) Representative confocal images of in toto immunolocalization assays revealed with an antibody conjugated with Alexa 488 -green fluorescence- and counterstained with propidium iodide -red fluorescence-. Control (a) and insulin (b), rapamycin (c) and metformin (d) treated metacestodes incubated with anti-TOR-P. Inset images correspond to transmission microscopy. Bars indicate 200 um. (B) Graph depicts the ratio of Em-TOR-PS3122 to nuclei fluorescence intensity in metacestodes treated with 1U/ml insulin (Ins), 10 uM rapamycin (Rp) and 10 mM metformin (Met) relative to controls (C). Values are expressed as means ± SEM (*p < 0.05 compared to control).
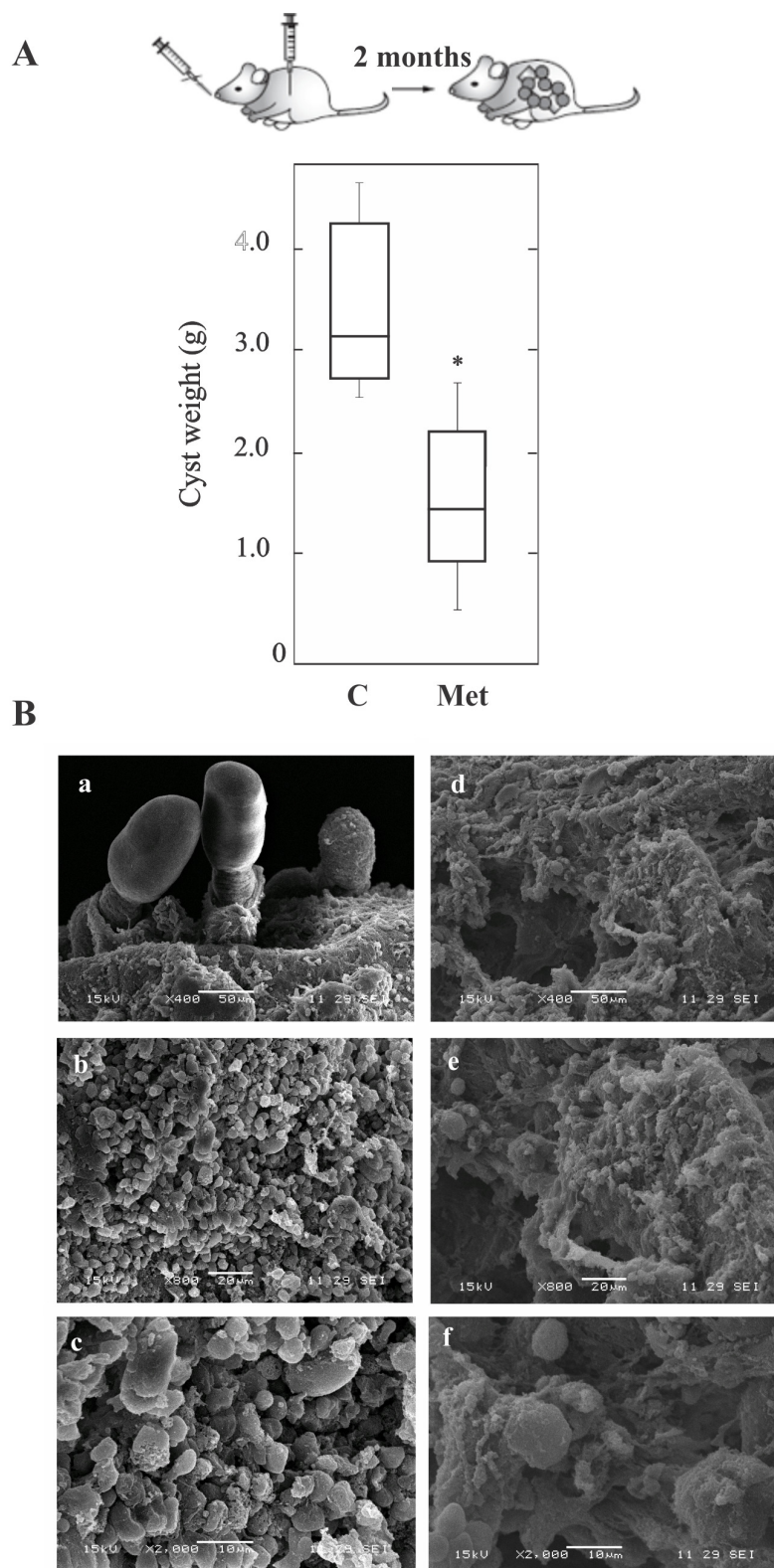
Figure 4. *In vivo* efficacy of metformina against *E. multilocularis* larva stage. Box plot showing the comparative distribution of the weight (g) of cysts recovered from untreated (C) and metformin-treated (Met, 50 mg/kg/d) mice. A significant cyst weight reduction (*$p < 0.05$) was achieved in treated animals. (B) Representative SEM images of cysts recovered from untreated control mice (a-c) compared with Met-treated mice (d-f). Bars indicate: 50 um in (a, d), 20 um in (b, e) and 10 um in (c, f).